3422–3436 *Nucleic Acids Research, 2017, Vol. 45, No. 6* *Published online 24 November 2016*
doi: 10.1093/nar/gkw1043

Spliceosomal protein eftud2 mutation leads to p53-dependent apoptosis in zebrafish neural progenitors

Lei Lei†, Shou-Yu Yan†, Ran Yang, Jia-Yu Chen, Yumei Li, Ye Bu, Nannan Chang, Qinchao Zhou, Xiaojun Zhu, Chuan-Yun Li* and Jing-Wei Xiong*

Institute of Molecular Medicine, Beijing Key Laboratory of Cardiometabolic Molecular Medicine, and State Key Laboratory of Natural and Biomimetic Drugs, Peking University, Beijing 100871, China

Received July 31, 2015; Revised October 19, 2016; Editorial Decision October 20, 2016; Accepted October 24, 2016

ABSTRACT

Haploinsufficiency of EFTUD2 (Elongation Factor Tu GTP Binding Domain Containing 2) is linked to human mandibulofacial dysostosis, Guion-Almeida type (MFDGA), but the underlying cellular and molecular mechanisms remain to be addressed. We report here the isolation, cloning and functional analysis of the mutated *eftud2* (*snu114*) in a novel neuronal mutant *fn10a* in zebrafish. This mutant displayed abnormal brain development with evident neuronal apoptosis while the development of other organs appeared less affected. Positional cloning revealed a nonsense mutation such that the mutant *eftud2* mRNA encoded a truncated Eftud2 protein and was subjected to nonsense-mediated decay. Disruption of *eftud2* led to increased apoptosis and mitosis of neural progenitors while it had little effect on differentiated neurons. Further RNA-seq and functional analyses revealed a transcriptome-wide RNA splicing deficiency and a large amount of intron-retaining and exon-skipping transcripts, which resulted in inadequate nonsense-mediated RNA decay and activation of the p53 pathway in *fn10a* mutants. Therefore, our study has established that *eftud2* functions in RNA splicing during neural development and provides a suitable zebrafish model for studying the molecular pathology of the neurological disease MFDGA.

INTRODUCTION

Most eukaryotic precursor mRNAs contain intronic sequences that are normally removed by splice machinery. The major spliceosome in the nucleus recognizes canonical consensus sequences (1,2) while the minor spliceosome recognizes non-canonical consensus sequences. Nonsense-mediated mRNA decay (NMD) is a widely-conserved mechanism to remove transcripts containing a premature termination codon, which is often found in aberrant RNA splice products (3–6).

U5 snRNPs (small nuclear ribonucleoprotein particles) are necessary for both the major and minor spliceosome machinery in conformation remodeling, a key stage in spliceosome activation (7–9). Eftud2 (elongation factor tu GTP binding domain containing 2, also called Snu114), a core component of U5 snRNPs, is a GTPase (10). Binding of GTP/GDP to Eftud2 plays a pivotal role in spliceosome dynamics (11). Disrupting the GTP binding domain of Eftud2 in *Saccharomyces cerevisiae* results in unspliced mRNAs and lethality (12), suggesting an irreplaceable role of *eftud2* in RNA splicing.

Several studies have reported that haploinsufficiency of EFTUD2 is linked to mandibulofacial dysostosis, Guion-Almeida type (MFDGA) (13–20), a syndrome characterized by microcephaly, midface hypoplasia, micrognathia and an abnormal appearance of the external ear (18). However, it remains to be addressed how EFTUD2 mutations cause the multiple neurological symptoms in MFDGA patients.

The zebrafish is a wonderful vertebrate model for studying neurogenesis (21,22). Neural stem cells are self-renewing cells that have the potential to generate neurons, astrocytes and oligodendrocytes (23–25). Zebrafish neural development starts at the gastrulation stage (26). SoxB1 family member Sox2 is enriched in neural progenitors and is required for their maintenance (27–29). During late gastrulation, neural progenitors start to express pro-neuronal genes, such as the basic helix–loop–helix-containing neurogenin1 (*ngn1*), which promotes the differentiation of neuronal progenitors (30,31). Shortly after gastrulation, intermediate filament *nestin* starts to appear in neural progenitors (32). After division and migration, neural progenitors exit from the

*To whom correspondence should be addressed. Tel: +86 10 62766239; Fax: +86 10 62767143; Email: jingwei_xiong@pku.edu.cn
Correspondence may also be addressed to Chuan-Yun Li. Email: chuanyunli@pku.edu.cn
†These authors contributed equally to this work as first authors.

cell cycle and form young post-mitotic neurons that express Elavl3 (ELAV-like neuron-specific RNA binding protein 3, also known as HuC) (31). Gliogenesis proceeds during neurogenesis, when the cytoskeletal protein glial fibrillary acid protein (GFAP) is mainly expressed in mature astrocytes (33). The balance of neural progenitors undergoing proliferation, differentiation, and/or programmed cell death ensures proper populations of each type of cell in the central nervous system (CNS) (24,25,31,34).

Here, we report the isolation and cloning of a novel zebrafish mutant, *fn10a*, that showed abnormal neurogenesis during early development, a phenotype recapitulating that of MFDGA patients. Positional cloning revealed that the spliceosomal gene *eftud2* was mutated in this mutant. Further molecular analyses revealed that *eftud2* is required for neuronal progenitor development by regulating the transcriptome-wide splicing of transcripts, particularly in the p53 and cell-cycle pathways. Therefore, *eftdu2*^{fn10a} allowed us, for the first time, to determine the function of *eftud2* in neuronal progenitor development and provides a suitable animal model for further determining the molecular pathology of MFDGA.

MATERIALS AND METHODS

Zebrafish husbandry

fn10a mutant and wild-type TL and WIK zebrafish were raised in an aquarium system at 28.5°C based on the 'IMM-XiongJW-3′ protocol that was approved by the Peking University Institutional Animal Care and Use Committee, which is fully accredited by the Association for Assessment and Accreditation of Laboratory Animal Care.

Positional cloning of the *fn10a* locus

fn10a was isolated in an ethylnitrosourea-induced mutagenesis screen for zebrafish cardiovascular mutants in the TL background at the Cardiovascular Research Center, Massachusetts General Hospital, Boston, MA. The genetic mapping strain *fn10a*/WIK was created by crossing heterozygous *fn10a* with wild-type WIK zebrafish. Phenotypically wild-type and mutant embryos were collected from pairwise mating of heterozygous *fn10a*/WIK zebrafish and scored for the brain apoptosis phenotype and pericardial edema at 48 hpf. Genomic DNA was isolated from individual *fn10a* mutants and their siblings (either genotypically wild-type or heterozygous for *fn10a*). The *fn10a* locus was mapped to Chromosome 3 using 500 simple sequence length polymorphism (SSLP) markers that were generated in the Fishman Laboratory at Massachusetts General Hospital, Boston (35). Further chromosome walking was performed by amplifying SSLP sequences and SSLP-based genotyping with 3300 meioses of mapping DNA. We carried out Sanger sequencing of genomic DNA and mRNA to identify the defective gene *eftud2* in the *fn10a* mutant locus. This mutation was further confirmed by the lack of Eftud2 in *fn10a* mutants in western blots, rescuing the *fn10a* mutant phenotype with *eftud2* mRNA, and phenocopying the *fn10a* mutant phenotype with *eftud2* morphants.

Construction and injection of neural progenitor reporters

The neuronal-glial reporter plasmid clone *gfap*-EGFP (36) was kindly provided by Dr Jiulin Du (Shanghai Institute for Biological Sciences, Shanghai). The neuronal progenitor reporter 6.9 kb *ngn1*-EGFP was constructed as described (37). Plasmids (30 ng/μl) were injected into *fn10a* mutants and siblings at the one-cell stage. Injected embryos were cultured at 28.5°C until they were harvested and fixed at the indicated time points.

cRNA and morpholino injections

The *upf1*, *eftud2* and *eftud2*^{fn10a} coding sequences were amplified from wild-type or *fn10a* mutant cDNA libraries, and then cloned into the pCS2+ vector using ClaI and SnaBI restriction endonucleases. Capped mRNAs of *upf1*, *eftud2* and *eftud2*^{fn10a} were synthesized using SP6 RNA polymerase (mMESSAGE mMACHINE® Kit, Ambion, Austin, TX, USA). *eftud2* or *eftud2*^{fn10a} mRNA (230 pg) was injected into embryos at the one-cell stage from mating crosses with heterozygous *fn10a* zebrafish, and injected embryos were scored for the mutant phenotype at 36 h post-fertilization (hpf). An ATG morpholino (MO) for *eftud2* was designed by and purchased from Gene Tools LLC (Philomath, OR) and the *p53*-MO and *upf1*-MO were as previously reported (38). The sequences of the *p53*-MO, *eftud2*-MO, and *upf1*-MO are listed in Supplementary Table S3. Eftud2-MO and/or *upf1* mRNA were injected into wild-type embryos at the one-cell stage, and injected embryos were collected at 36 hpf for isolation of total RNA and quantitative RT-PCR.

In situ hybridization

Whole-mount *in situ* hybridization was performed as previously described (39). PCR fragments for *tuba*, *nestin*, *map2*, *eftud2*, *foxa3* and *wt1a* were amplified from a 48 hpf embryonic cDNA library and confirmed by Sanger sequencing; the T7 RNA polymerase binding site was introduced to make anti-sense RNA probes. Digoxigenin-labeled probes were synthesized using T7 RNA polymerase (Roche). The RNA probes of *pax2a*, *myoD*, *cmyb*, *lyzC*, *amhc* and *vmhc* were synthesized as previously reported (40).

Immunostaining, cryosections, and apoptosis assay

For whole-mount immunostaining, embryos at 36 and 48 hpf were fixed in 4% paraformaldehyde (41) for 30 min and then digested in 10 μg/ml proteinase K for 40 min. For immunostaining of cryosections, embryos at 36 and 48 hpf were fixed in 4% PFA, washed in phosphate-buffered saline plus Tween-20 (PBST), embedded in 25% sucrose for 1 h, and then transferred to 35% sucrose at 4°C overnight. Embedded embryos were transferred into optimal cutting temperature (OCT) compound. Cryosections of the brain (4 μm) and the spinal cord (10 μm) were cut on a microtome (Leica, Wetzlar, Germany). The following antibodies were used: anti-mouse Huc (1:100, Invitrogen 16A11), anti-rabbit Sox2 (1:200, Abcam #ab997959), anti-mouse GFAP (1:50, Sigma 083M4785), anti-rabbit pH3 (1:100, Millipore

2066052), Alexa Fluor 555 goat anti-rabbit IgG2b (1:200, Invitrogen), Alexa Fluor 488 goat anti-mouse IgG2b (1:200, Invitrogen), and Alexa Fluor 633 goat anti-rabbit IgG2b (1:200, Invitrogen). Cell death was assessed by TUNEL staining using the DeadEnd™ Fluorometric TUNEL System (Promega) and an *in situ* cell death detection kit (TMR red, Roche).

Western blot

Protein samples were isolated from 36 hpf *fn10a* mutants and siblings. The yolk was removed by pipetting with 21G needles in PBS containing complete protease inhibitors (42). The embryos were ground and incubated in RIPA lysis buffer with protease and phosphatase inhibitors (42). Anti-Eftud2 (1:1000, Sigma HPA022021), anti-tubulin (BE0031, EASYBIO) and anti-β-actin (1:1000, Cell Signaling 4967L) were used for western blots as previously described (40).

RNA-Seq library preparation, sequencing and mapping

Total RNA of 36 hpf *fn10a* mutants (mutant group) and siblings (WT-sibling group) were isolated using Trizol reagent (Sigma). Each sample containing 30 embryos was used for RNA-Seq assays and real-time PCR. To prepare cytoplasmic and nuclear RNA, embryos were collected and dechorionated at 36 hpf. The yolk was removed by pipetting with PBS containing complete protease inhibitors (42) using 21G needles. The cytoplasmic and nuclear fractions were then separated with a PARIS kit (AM1921, Life Technologies). Aliquots of the cytoplasmic and nuclear lysates were saved for western blot analysis. RNA was isolated by mixing cytoplasmic or nuclear lysate with the lysis/binding solution and purified using a filter cartridge. Purified RNAs were incubated with DNase I for 30 min at 37°C to remove residual genomic DNA and purified again using an RNAeasy kit (74104, Qiagen). Aliquots of nuclear and cytoplasmic RNAs were saved for quality testing by RT-PCR. RNA-Seq assays were performed by the Beijing Genome Institute (BGI, Shenzhen). The wild-type control group (WT-control group) of 36-hpf embryos was generated from mating crosses between wild-type TL zebrafish. We used the deoxy-UTP approach to prepare strand-specific libraries as previously reported (43). RNA-Seq was performed on an Illumina HiSeq2000 platform. Nuclear and cytoplasmic RNA-seq was performed under a standard protocol in BIOPIC, Peking University. RNA-Seq reads were mapped on the Zebrafish Genome Sequence (Zv9) by Tophat (v2.0.8). Our in-house evaluation pipeline implemented a series of Perl (v5.12.2), Python (v2.7.5) and R (v2.13.1) scripts to assess the quality of the RNA-seq experiments (44). RefSeq gene structure data were downloaded from the ftp site of the UCSC genome browser on 2014.1.12. RNA-seq data in this study have been uploaded to GEO under accession number GSE78106.

Calculation of splicing efficiency

Similar to the exonic inclusion ratio 'percent spliced in', we named the intronic exclusion ratio 'percent spliced out' (PSO) (45). The value of PSO, which varies between 0 and 1 for evaluating the proportion of junction reads, was calculated as the percentage of correct splicing from the total junction reads. We mapped RNA-Seq reads using Tophat2 to elicit the anchoring problem, i.e. several bases of junction reads mapped to an intron.

Identification and characterization of abnormally retained introns in *fn10a* mutants

To identify intron retention (IR) in *fn10a* mutants, we counted the number of junction reads supporting IR or excision in the WT-sibling, WT-control and *fn10a* mutant groups. Then we performed Fisher's exact test on the 2 × 2 contingency table. Introns with a false-discovery rate (FDR) corrected *P*-value <0.001 in both mutant versus WT-sibling and mutant *vs* WT-control were further identified as described (46). Briefly, for each intron, we counted the median coverage of introns and its flanking exons, and then performed statistical inference as described (47). Introns with FDR corrected *P*-values <0.001 were identified as statistically affected. Genes were clustered using DAVID (http://david.abcc.ncifcrf.gov/) for functional enrichment analysis.

We divided all introns of RefSeq transcripts into three groups: the 653 most severely retained introns found previously (retIntron), other introns in the 484 affected genes (retGenes Other introns), and introns in other RefSeq genes (refGenes). For each group, we calculated the GC content in five regions: the 5′ exon, 30 bp of intron adjacent to the 5′ exon, the intron, 30 bp of intron adjacent to the 3′ exon, and the 3′ exon. We compared the splicing strength by maximum entropy modeling of short sequence motifs in the three groups of introns defined above (48).

RNAscope *in situ* hybridization

Embryos were collected at 36 hpf and fixed in 4% PFA for 45 min at room temperature. Whole-mount *in situ* hybridization was performed using an RNAscope (BROWN) kit (320497, Advanced Cell Diagnostics, ACD) as described (49). For cryosections, fixed embryos were impregnated with 15%, 25% and 35% sucrose, then frozen in OCT embedding medium, and sections were cut at 10 μm. Fluorescent *in situ* staining was performed according to the user's manual supplied by ACD (320293, Advanced Cell Diagnostics). The intron-containing probes *ccnb1* (intron 3, chr5:54090296-54091076) and *tardbp* (intron 2, chr6:45937988-45938509) were designed by ACD and the control probes *odc1* and *dapB* were provided by ACD.

Statistical inference of differential gene expression

Differential expression was assessed using R package DEGseq (50). We defined genes with expression fold changes ≥2 and FDR adjusted *P*-values <0.001 as significant. Differentially expressed genes were clustered by DAVID for functional enrichment analysis.

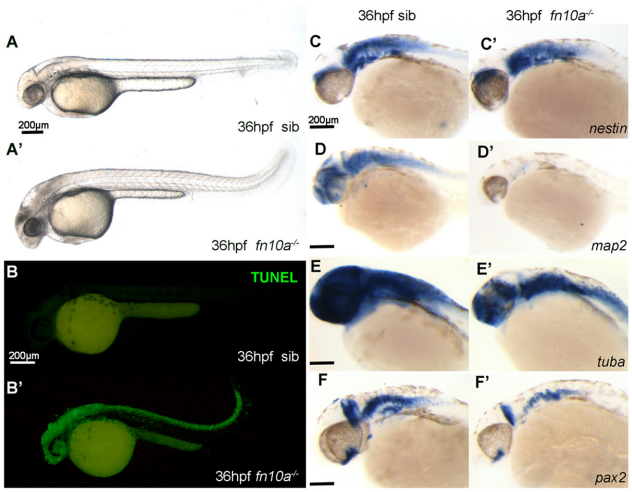

Figure 1. The CNS and spinal cord undergo apoptosis and fail to differentiate in *fn10a* mutants. (A, A) An *fn10a* mutant (**A**) showing morphological defects in the brain and tail compared with a wild-type sibling (sib) embryo (A). (B, B') TUNEL staining showing that the *fn10a* mutant (**B**) had severe apoptosis in the CNS and neural tube. (C–F, C'–F') *In situ* staining for neural markers revealed that differentiated neuronal markers (D–D', *map2*; E–E', *tuba*; F–F', *pax2*) but not a neural progenitor marker (C–C', *nestin*) were affected in *fn10a* mutants (**C–F**) compared with those in their siblings (C–F). Scale bars, 200 μm. The number of embryos assayed was ≥13 for each panel.

RESULTS

The *fn10a* mutant has severe defects in the CNS and spinal cord

As a part of a study of ethylnitrosourea-induced mutagenesis of the zebrafish genome, we isolated the novel neuronal mutant *fn10a*. This mutant had a smaller head, abnormal brain development with a number of dead cells in the head region, and a curled-up tail by 36 hpf (Figure 1A') compared with wild-type siblings (Figure 1A). TUNEL assays revealed that apoptotic cells were primarily located in the CNS and spinal cord of *fn10a* mutants (Figure 1B') compared with their wild-type siblings at 36 hpf (Figure 1B). We then tested whether neuronal development is interrupted in this mutant. Whole-mount RNA *in situ* hybridization was performed with RNA probes for the neuronal progenitor marker *nestin*, newly-formed neuronal marker *map2*, mature neuronal marker *tubulina* (*tuba*), and the neuronal patterning marker *pax2*. Intriguingly, *nestin* was normally expressed (Figure 1C') while *map2*, *tuba* and *pax2* were all down-regulated in *fn10a* mutants (Figure 1D'–F') compared with their wild-type siblings (Figure 1C–F). These data suggested that neuronal differentiation is disrupted, probably due to neuronal progenitor apoptosis in *fn10a* mutants.

Positional cloning identifies *eftud2* as the defective gene in the *fn10a* locus

Positional cloning was performed to determine the molecular nature of the mutations in *fn10a* mutants. The *fn10a* locus was first mapped to Chromosome 3 by using 500 SSLP markers. Bulk segregation analyses narrowed the *fn10a* locus to a 200-kb interval between markers 10j-9 and 219o-30 (Figure 2A). By sequencing the exons of genes in this interval, we found a C-to-T mutation in exon 24 of *eftud2*, which caused a premature stop codon at Q808 (Figure 2B; arrow). Comparing the cDNA sequences of the mutant (T) and wild-type (C) alleles in heterozygous *fn10a* mutants, we found that the mutant allele appeared to be much less abundant (Figure 2C; right panels), while the genomic DNA sequences of both mutant and wild-type alleles were equal (Figure 2C; left panels). This result was verified by western blots showing that Eftud2 proteins were undetectable in *fn10a* mutants (Figure 2D). These results suggested that *fn10a* mutant transcripts are not stable, probably due to NMD. To confirm that *eftud2* was the mutated gene in *fn10a*, we injected one-cell embryos with either $eftud2^{fn10a}$ or wild-type *eftud2* mRNA, and then carried out TUNEL assays. Consistently, >80% of the *fn10a* mutants were rescued to decrease TUNEL-positive cells by wild-type *eftud2* mRNA, but <20% by $eftud2^{fn10a}$ mutant mRNA (Figure 2E). The mutant phenotype that was partially rescued by the $eftud2^{fn10a}$ mutant mRNA further suggested that the truncated $Eftud2^{fn10a}$ protein has partial function but its mRNA is not stable. Together, these genetic and epistatic analyses showed that *eftud2* is the mutated gene in the *fn10a* locus.

Zebrafish Eftud2 is highly conserved, its human homolog EFTUD2 showing 91.5% sequence identity in amino acids (Supplementary Figure S1). Eftud2 is known to be one component of the spliceosome, and plays a key role in spliceosome remodeling (10,11). To address *eftud2* function in zebrafish neuronal development, we began by examining the expression pattern of *eftud2* during embryogenesis. Whole-mount RNA *in situ* hybridization revealed that *eftud2* was widely expressed at early stages (from 3 to 16 hpf) and gradually concentrated in the brain and eyes from 24 to 48 hpf, suggesting that *eftud2* is a sustained requirement for brain development (Figure 2F). Since *eftud2* was widely expressed at early stages, we tested whether other organ patterning and/or development were affected in this mutant. To our surprise, the majority of organ-specific markers tested were not or little affected in *fn10a* mutants, including the skeletal-muscle marker *myoD*, which was normally expressed in somites (Supplementary Figure S2A, A'); macrophage-specific *lysozyme C* was slightly reduced (Supplementary Figure S2B, B'); the definitive hematopoietic marker *cmyb* appeared to be normal (Supplementary Figure S2C, C'); the digestive organ-specific marker *foxa3* was normally expressed, except for less in the pancreas (Supplementary Figure S2D, D'); the kidney-specific markers *pax2* and *wt1a* were normal (Supplementary Figure S2E, E', S2F, F'); and ventricle-specific myosin heavy-chain (*vmhc*) and atrium-specific myosin heavy-chain (*amhc*) were also normally expressed, although cardiac looping was defective (Supplementary Figure S2G, G', S2H, H'). Together, these results suggested that Eftud2 plays an essential role in neuronal development while it has little or no function in the development of other organs.

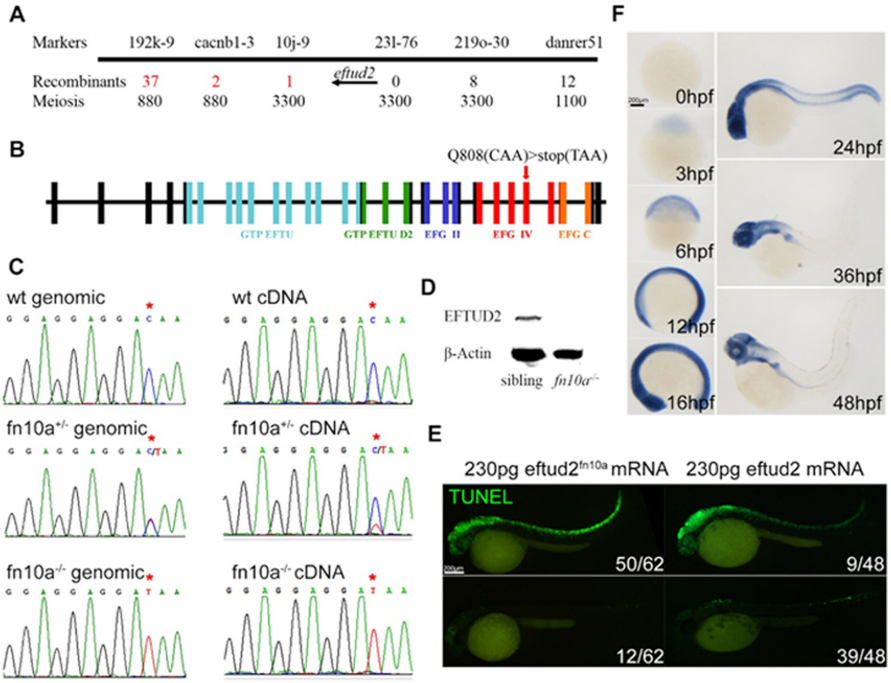

Figure 2. The *fn10a* locus encodes Eftud2 in zebrafish. (**A**) Regional fine-map of *fn10a* with the flanking genetic markers in chromosome 3, showing that *eftud2* is located between genetic markers 10j-9 and 231–276. (**B**) A C-to-T mutation in exon 24 led to premature termination of *eftud2* translation that produced mutant Eftud2 protein lacking 165 amino-acids in the C-terminus. (**C**) Sequencing data of genomic and cDNA of wild-type sibling, heterozygous, and mutant *fn10a* embryos. Note that mutant *eftud2* mRNA is not stable in *fn10a*$^{+/-}$ mutants. (**D**) Western blot showing that Eftud2 protein was not detectable in *fn10a*$^{-/-}$ mutants. β-Actin was used to normalize protein loading. (**E**) Left panels: TUNEL staining for neuronal apoptosis in only 12/68 *fn10a* mutants was rescued (lower panel) while that in 50/62 mutants was not rescued (upper panel) by mutant *eftud2*^{fn10a} mRNA. Right panels: TUNEL staining for neuronal apoptosis in 39/48 *fn10a* mutants was rescued (lower panel) but that in 9/48 mutants was rescued less (upper panel) by wild-type *eftud2* mRNA. All *fn10a* mutants were confirmed by PCR-based genotyping. (**F**) Whole-mount *in situ* hybridization revealed that *eftud2* was broadly expressed at 3, 6, 12, 16 and 24 hpf and enriched in the brain and branchial arches at 36 and 48 hpf. Scale bar, 200 μm.

Eftud2 is required for the maintenance and differentiation of neuronal precursors

To address which cell types in the brain and spinal cord were affected in *eftud2* mutant embryos, we determined the co-localization of TUNEL$^+$ apoptotic cells and neuronal/glial cells by immunostaining for the neuronal progenitor marker Sox2, the immature post-mitotic neuronal marker Huc, and the glial marker GFAP (Figure 3). From 36 to 48 hpf, apoptotic cells stained by TUNEL were well co-localized with Sox2 in the brain (Figure 3B, B') and spinal cord (Figure 3M', N') of *fn10a* mutants compared with wild-type siblings (Figure 3A, A', C, C', M, N). However, apoptotic cells overlapped less with Huc and Gfap in the brain (Figure 3F, F') and spinal cord (Figure 3O', P', Q', R'). These results suggested that *eftud2* is required for the survival of neural progenitors rather than differentiated neurons. Besides, the neurons and glia labeled by Sox2, Huc or Gfap in the spinal cord were severely deformed, suggesting an arrest of neural fate shift during early development (Figure 3M-R and M'-R'). To confirm the above results, we used the neuronal progenitor reporter *ngn1*:GFP and neuronal-glial cell reporter *gfap*:GFP for more sensitive labeling of these lineages (36,37). Consistently, *ngn1*:GFP$^+$ cells were co-localized with apoptotic cells, but *gfap*:GFP$^+$ cells rarely underwent apoptosis (Supplementary Figure S3). Together, these results suggested that mutation of *eftud2* leads to apoptosis in neural progenitors and the subsequent disruption of neural differentiation.

We then asked whether the proliferation of neuronal progenitors was affected in *fn10a* mutants. The mitotic phase marker phosphorylated histone 3 (pH3) was used to label proliferating cells. Co-staining for pH3 and TUNEL at 36 hpf revealed that mitotic neuronal progenitors rarely underwent apoptosis in the brain (Figure 3J, L and J', L') and spinal cord (Figure 3S'–T', and U'–V') in *fn10a* mutants. However, at 48 hpf, increased numbers of proliferating neural progenitors were undergoing apoptosis in *fn10a* mutants, accompanied by abnormal chromosome segregation in most pH3-positive nuclei in both the brain (Figure 3L, L′) and spinal cord (Figure 3T′, V′), consistent with a previous report that knockdown of *eftud2* in HeLa cells leads to metaphase alignment problems and consequently mitotic exit arrest, mitotic cell accumulation and cell death (51). These data suggested the occurrence of a burst of neural progenitor proliferation accompanied by the loss of these progenitors due to cell-division problems and apoptosis, probably reflecting a feedback mechanism in *fn10a* mutants.

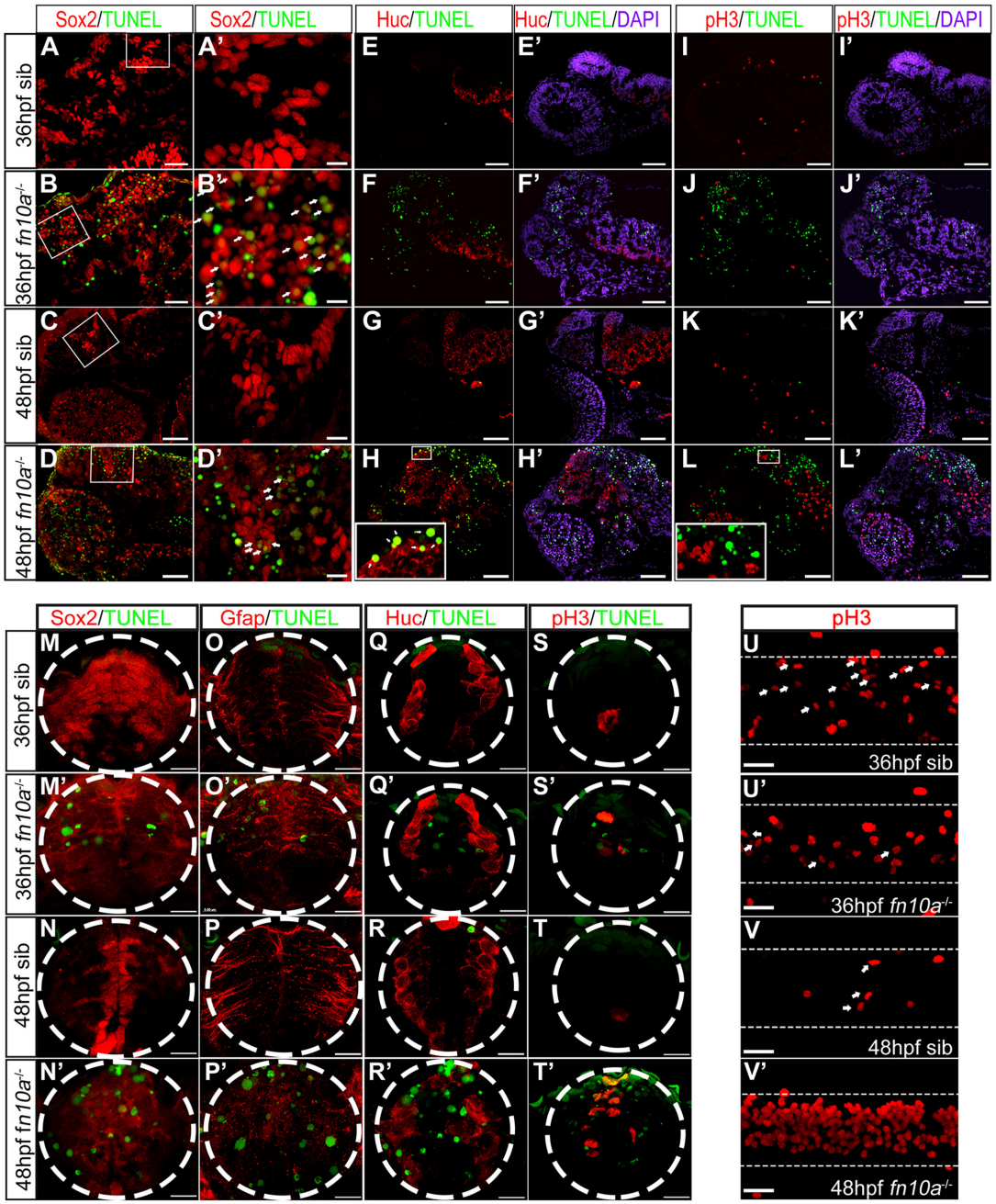

Figure 3. Neuronal progenitors undergo apoptosis in both the head and spinal cord of *eftud2*^{fn10a} mutants. Immunostaining and TUNEL staining in cryosections of the embryonic brain (A–L, A'–L') and spinal cord (M–T, M'–T') at 36 and 48 hpf. (A–D, A'–D') The neural progenitor marker Sox2 was co-localized with apoptotic (TUNEL^{+}) cells in *fn10a* mutants (B, B', D, D'). Panels A' to D' are expanded from the boxed areas in panels (A to D). Apoptotic cells were hardly detectable in wild-type siblings (A, A', C, C'). (E–H, E'–H') The postmitotic neuronal marker Huc at 36 hpf was not co-localized (F, F'), but was partially co-localized at 48 hpf (H, H') with apoptotic cells in *fn10a* mutants. (I–L, I'-L') The mitotic-phase marker pH3 was barely co-localized with apoptotic cells in *fn10a* mutants at 36 hpf and 48 hpf. Note that the number of pH3^{+} cells was dramatically higher in *fn10a* mutants at 48 hpf (L, L') than at 36 hpf (J, J'). (M–N') The neuronal precursor marker sox2 was co-localized with apoptotic cells in the spinal cord in *fn10a* mutants. Note more TUNEL-positive cells in *fn10a* mutants (M', N'). (O–P') Immunostaining revealed the disruption of neural-glial cell formation with more TUNEL-positive cells in *fn10a* mutants (O', P') than in sibling controls (O, P). (Q–R') Newly-generated Huc^{+} neurons were less affected in *fn10a* mutants at 36 hpf (Q'), but they underwent apoptosis at 48 hpf (R'). (S–T', U–V') The mitotic-phase marker pH3 was increased in *fn10a* mutants at 48 hpf and partially overlapped with apoptotic cells (S', T'). (M–T') Transverse views; (U–V') sagittal views. Scale bars in A–D, E–L', 50 μm; A'–D', M–T', 10 μm; U–V', 30 μm; $n \geq 5$ for each panel.

Transcriptome-wide splice efficiency is compromised in *eftud2*^{fn10a} mutants

We then used RNA-seq to investigate how disrupting *eftud2* affected the transcriptome in *fn10a* mutants. We compared the transcriptomes in *fn10a* mutants (−/−), wild-type *fn10a* siblings (+/− and +/+), and a wild-type controls (+/+) at 36 hpf (Supplementary Figure S4). To characterize mRNA structures accurately, we adopted a strand-specific poly(A)-positive strategy and generated 413.7 million 100-bp paired-end reads in total. Among these, 330.5 million reads were uniquely mapped to the zebrafish genome (Zv9/danRer7), of which nearly 30% (98.3 million) reads had one or more junctions.

We assessed the capacity for intron removal, i.e. the splicing efficiency, in *fn10a* mutants. Similar to the parameter 'percent spliced in' for exons, the intron-centered index PSO was calculated to assess the splicing efficiency for each intron as previously described (45). The PSOs in *fn10a* siblings (+/− and +/+) and wild-type controls (+/+) appeared to be comparable, suggesting that mutation in one allele of *eftud2* has no effect on RNA splicing in zebrafish. In contrast, we found a transcriptome-wide decrease of splicing efficiency in *fn10a* mutants. Binning introns in mutants according to their PSOs, we found that, no matter whether the value for each bin was low or high, the corresponding PSO values were lower in the mutant group than those in both the sibling and wild-type groups (Figure 4C). By selecting 10 introns, of which seven were from seven different genes and three from one randomly-selected gene (NM_130955), we confirmed their IR in *fn10a* mutants by RT-PCR (Figure 4H; Supplementary Figure S5). The same IR transcripts were also found in *eftud2* morphants (Supplementary Figure S5). Thus, mutation of *eftud2* had a major impact on the transcriptome by generating a large amount of IR transcripts. Importantly, the intron-containing transcripts *ccnb1* and *tardbp* were enriched in the mutant brain (Supplementary Figure S6C'–D'), consistent with the major defects in the CNS of this mutant (Figures 1 and 3). In particular, *ccnb1* (also called cyclin B1) is a cell-cycle kinase necessary for the G2/M transition, and *tardbp* (also called TAR DNA binding protein) is required for RNA splicing and is a causative gene in some neurodegenerative disorders (52). Considering that NMD can eliminate aberrant transcripts (53,54), we reasoned that there would be more IR transcripts than those that we were able to identify, since a fraction of them were degraded immediately in *fn10a* mutants.

Eftud2 mutation leads to aberrant intron-retention and exon-skipping

Since splicing efficiency was compromised by *eftud2* mutation, we anticipated to find aberrant splicing events and related features in *fn10a* mutants. We hypothesized that the abnormalities of U5 snRNP would impact on splicing regulation and such impact might be selective between transcripts according to certain criteria. We first analyzed IR events. By comparing PSOs and intronic read coverage, we identified a group of 653 introns from 484 genes that had severe IR in *fn10a* mutants compared with either wild-type controls or *fn10a* siblings (Supplementary Figure S7 and Table S5). We then analyzed the *cis*-features of the most severely retained introns and found that they appeared to be shorter, with nearly 70% less than 500 bp (Figure 4D), and had a higher GC content (Figure 4E). In addition, the splicing strength of the three groups (wild-type controls, *fn10a* siblings, and *fn10a* mutants) had similar distributions at the 5′ motif, but differed at the 3′ motif (Figure 4F–G). The transcriptome-wide decrease of intron-removal efficiency and cis-features of the retained introns were independently confirmed by another biological replicate of RNA-seq (Supplementary Figures S8–S9 and Tables S9–S10).

It is known that under certain conditions, some introns are retained to fulfil their physiological functions (46,55). A recent report suggests that IR is a widespread, alternative splicing event in mammals. These introns are characterized by higher GC content, shorter length, weaker splice sites and other features (56). Together, our data further support the idea that *cis*-features are conserved (except for the 5′splicing strength) from zebrafish to mammals.

We then investigated exon-skipping (ES). We found almost twice as many ES events in *fn10a* mutants than in wild-type embryos and wild-type *fn10* siblings; 2217 ES events were mutant-specific (Figure 5A). Using a strategy similar to that for finding IR, we found 632 ES events (in 560 genes) that were differentially expressed in *fn10a* mutants and controls (Supplementary Table S11). To address whether these significantly changed ES events are associated with the decreased splicing efficiency, we calculated the degree of IR around them. As multiple splicing junctions occurred in ES events, read coverage had to be considered in order to clearly estimate the degree of IR. We used 'median coverage of introns divided by median coverage of flanking exons' to represent the IR level in thousandths (multiply by 1000). Interestingly, we found that the IR level was higher around the 632 significantly changed ES events in *fn10a* mutants (Figure 5B), suggesting that ES might be an alternative means of alleviating the impact of compromised splicing efficiency in this mutant.

It has been reported recently that many intron-containing transcripts are located in the nucleus of human cells, based on a global transcriptome analysis (57). To determine the localization of IR transcripts in *fn10a* mutants, we performed polyA$^+$ RNA-seq of nuclear and cytoplasmic fractions from *fn10a* mutant and wild-type sibling embryos at 36 hpf (Supplementary Figure S10A). We found that more intronic reads occurred in the nucleus than in the cytoplasm, and the proportion of intronic reads was highest in the mutant nucleus (Supplementary Figure S10B), consistent with the decrease of splicing efficiency in *fn10a* mutants. To address whether IR transcripts can be exported to the cytoplasm, we calculated the PSOs of introns in RefSeq genes for all 4 samples using the method described previously. We found a clear decrease of splicing efficiency in the mutant nucleus compared with the wild-type sibling nucleus. Besides, the splicing efficiency in the mutant cytoplasm was also significantly lower than that in wild-type siblings (Wilcoxon test P-value <2.2e-16), confirming the presence of IR transcripts in the cytoplasm (Supplementary Figure S10C). We checked the PSOs of the 653 severely retained introns in both the cytoplasm and nucleus; this showed a general trend of decreased splicing efficiency in this mutant

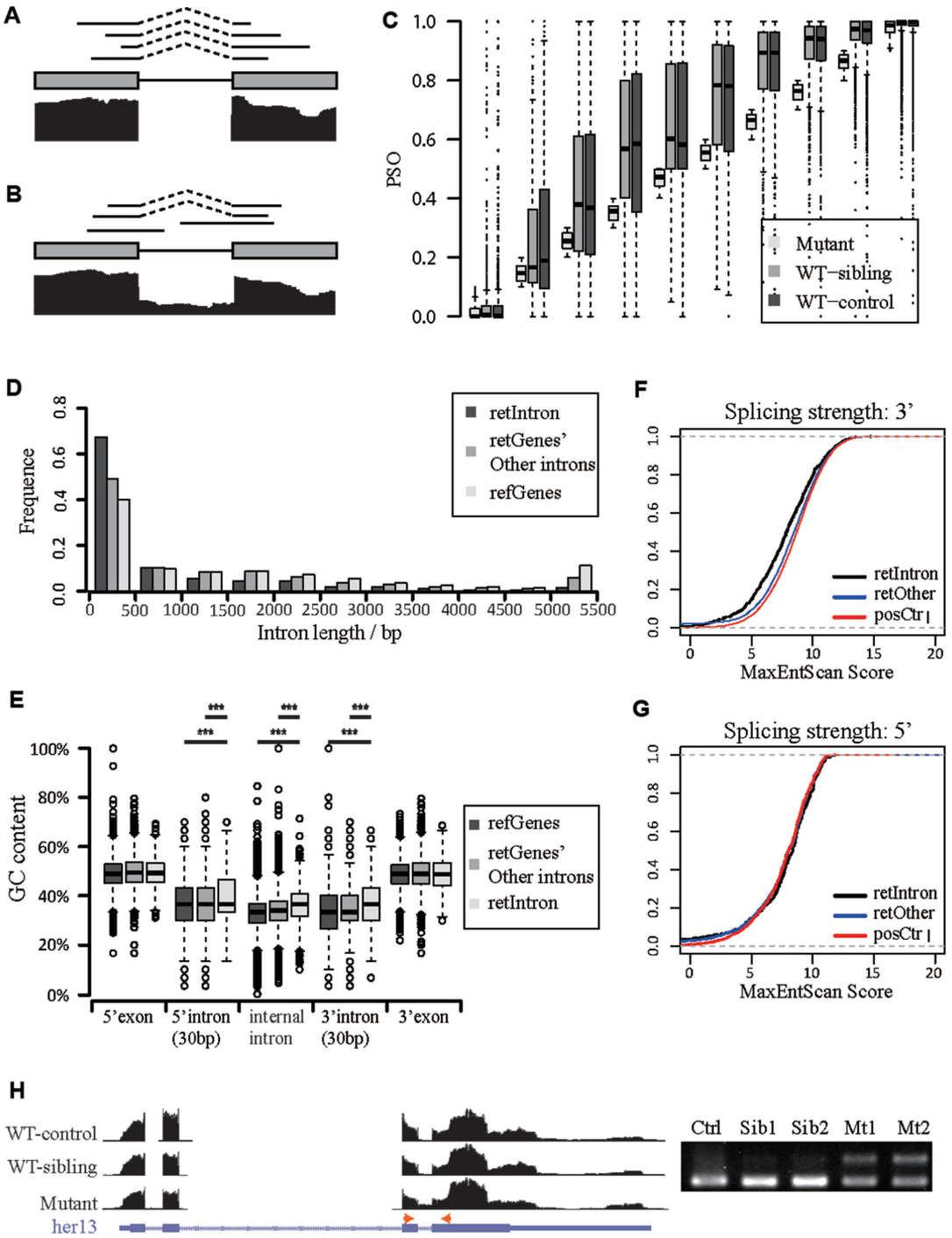

Figure 4. Transcriptome-wide decrease of splicing efficiency in *fn10a* mutant. (**A**) Schematic representation of a properly-spliced intron. Upper panel: all junction reads are mapped to the exon. Lower panel: reads only cover the exonic region. (**B**) Schematic representation of an intron with decreased splicing efficiency. Upper: some reads mapped to the exon-intron boundary come from intron-retaining transcripts. Lower: reads cover the intronic region as well as the exonic region. (**C**) Boxplot of PSO values for introns (with ≥10 junction reads) binned by its PSO in the mutant. For each bin, the mutant PSOs are lower than in its wild-type counterparts, indicating a global decrease of splicing efficiency. (**D**) Compared with other introns on the same gene (retGenes Other introns) or all RefSeq annotated introns (refGenes), severely retained introns (retIntron) were shorter and had a more right-skewed distribution. (**E**) The GC content of 'retIntrons' was higher in the intronic regions but similar in the flanking exons compared with those of 'refGenes' and 'retGenes other introns'. (**F–G**) The splice strength of 3′ splice sites (**F**), but not 5′ splice sites (**G**), was lower in 'retIntrons'. (**H**) A demonstration case of reduced intron-removing efficiency in this mutant. Left: gene structure and coverage in three samples. Right: RT-PCR using primers indicated by arrows.

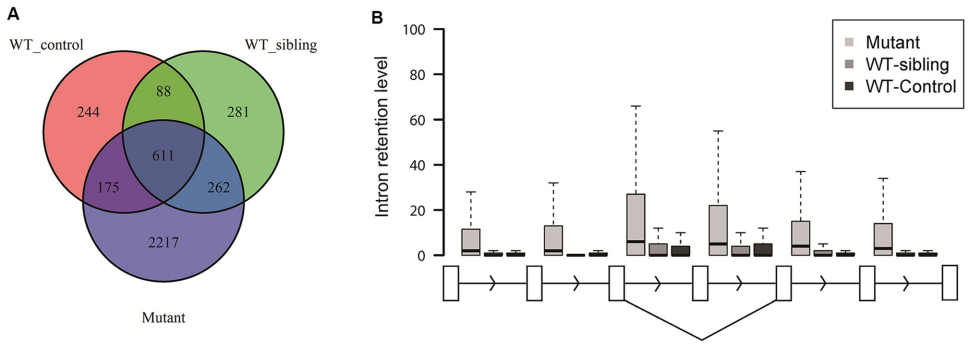

Figure 5. Exon-skipping (ES) events between *fn10a* mutant and wild-type controls. (**A**) ES occurs more frequently in mutants than in WT-controls or WT-siblings. (**B**) For ES events that significantly differed between mutants and controls ($n = 651$), the local 'intron-retention level' was higher in mutants. The intron retention level was calculated as the median coverage of introns divided by the median coverage of its flanking exons in thousandths; this reflects the degree of intron retention by considering not only junction sites, but also the internal coverage.

in both the cytoplasm and nucleus, only differing in degree (Supplementary Figure S10D-S10E). Importantly, by testing several IR transcripts with RNAscope *in situ* hybridization, we found that the intron-containing probes *ccnb1* and *tardbp* were higher in *fn10a* mutants (Supplementary Figure S11F', H') than in wild-type siblings (Supplementary Figure S11E', G'), and were located both in the cytoplasm and nucleus in the mutant (Supplemental Figure S11F", H"). Therefore, both RNA-seq and RNA *in situ* analyses support the notion that IR transcripts can be exported into the cytoplasm, although a large proportion remains in the nucleus of the mutant.

Nonsense-mediated mRNA decay partially counteracts and removes intron-retention and exon-skipping transcripts in *fn10a* mutants

Since mutation of *eftud2* results in large amounts of IR and ES transcripts, we reasoned that the NMD pathway, a prevalent and highly-conserved mechanism in the degradation of aberrant transcripts from zebrafish to mammals (3), might have been activated in *fn10a* mutants. In the 653 severely-retained introns, 505 induced premature stop codons, making them potential targets for NMD (Supplementary Figure S7 and Table S6). Among the 2217 mutant-specific ES events, nearly half (1095) generated premature stop codons upstream of the splicing junction (>55 bp), a feature of potential NMD targets (Supplementary Table S9). We directly detected 242 of these transcripts in the RNA-Seq data from mutant cytoplasmic RNA, suggesting that these mutant-specific isoforms are potential targets of NMD.

The abnormal and abundant IR/ES events in *fn10a* mutants suggested an unmet need for NMD. In another words, we hypothesized that the NMD mechanism was exploited to its maximum but still could not meet the need in *fn10a* mutants. If this assumption was true, the endogenous NMD targets would be partially relieved due to competition from other targets of NMD. Thus, we expected that the endogenous genes naturally under NMD regulation would be derepressed, that is, up-regulated in *fn10a* mutants (Figure 6A). To test this hypothesis, we selected two well-known and highly-conserved NMD target genes, *mmp30* and *atxn1b* (58). Inhibition of Upf1, the key component of NMD, by MO knockdown increased the expression levels of the two natural targets. Second, as we anticipated, qPCR showed that the two genes were also higher in *fn10a* mutants and *eftud2* morphants than in wild-type controls (Figure 6B). On the other hand, if we expanded the NMD capacity in the *fn10a* mutant, aberrant transcripts and natural NMD targets would be degraded more, and we would find a decrease in their expression. It has been reported that overexpression of *upf1* partially activates the NMD system (59). As expected, we found that the elevated expression of *atxn1b* and *mmp30* was reversed by *upf1* mRNA injection in *eftud2*^{fn10a} mutants (Figure 6B). In zebrafish, knockdown of *upf1* or other key components of NMD leads to multiple embryonic defects, especially in the brain (38,60). Therefore, the saturation of NMD in *fn10a* mutants presents an interesting phenotype similar to that in *upf1*-knockdown mutants.

To directly test whether the NMD mechanism is unable to remove the abnormal IR/ES transcripts, we compared the expression levels of IR- or ES-containing transcripts in the cytoplasm between *eftud2* morphants and *eftud2* morphants over-expressing *upf1* mRNA (Figure 6C–E). Consistently, we found that either IR or ES events were decreased in the cytoplasm of *eftud2* morphants when upf1 mRNA was over-expressed. Together, these data suggest that mutation of *eftud2* leads to a disruption of the mRNA splicing pattern, and subsequently creates large amounts of aberrant IR/ES transcripts that overwhelm the capacity of the NMD machinery.

The p53 pathway is activated to mediate neuronal apoptosis in *fn10a* mutants

To further explore how the splicing deficiency of the transcriptome leads to neural apoptosis in *fn10a* mutants, we systematically analyzed the 484 genes that contained the 653 most severely-retained introns (Supplementary Table S6). Intriguingly, the most severely intron-retaining genes were significantly enriched in several KEGG pathways, including the cell cycle, the p53 signaling pathway, and the spliceosome. By determining the expression patterns of the genes, we found that several were differentially expressed in

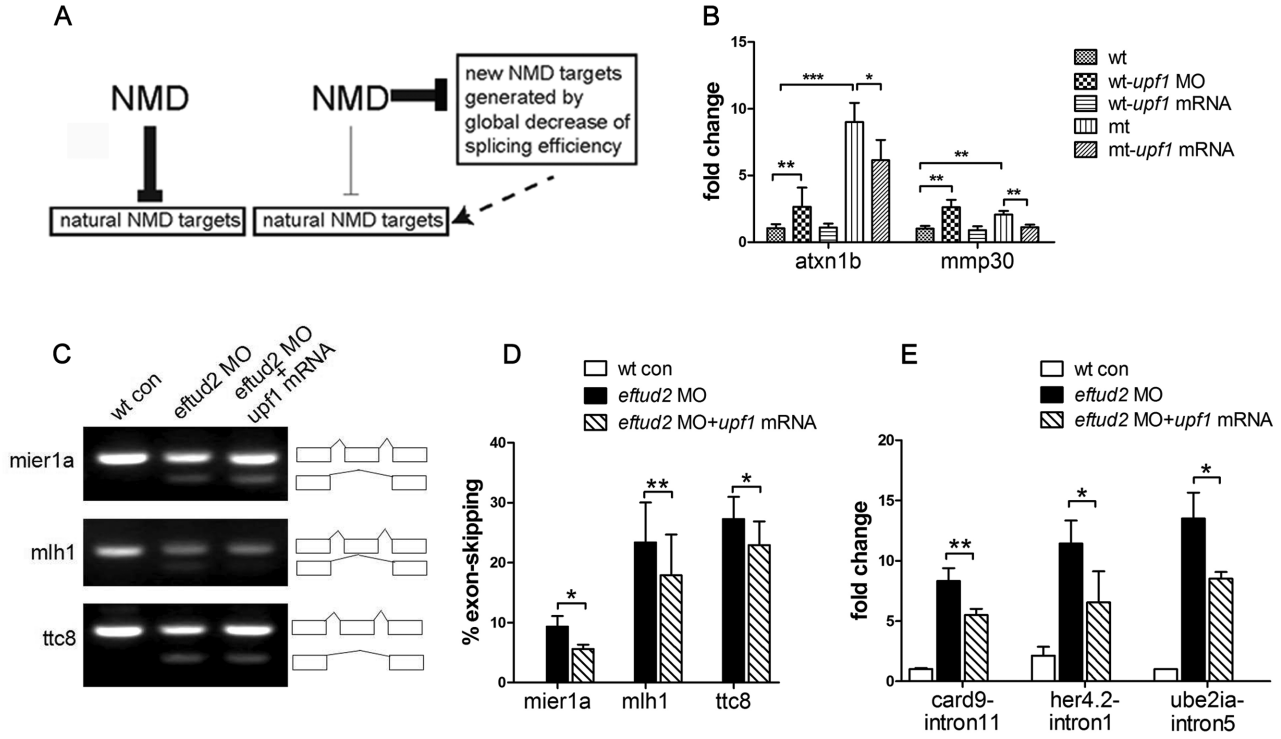

Figure 6. The endogenous NMD mechanism is compromised due to genome-wide deficiency of mRNA splicing in *fn10a* mutants. (**A**) Schematic of normal NMD and its targets in wild-type (WT) embryos, and abnormal NMD and its overload of targets in *eftud2*^{fn10a} mutants. It is hypothesized that mRNA splicing-deficiency leads to abnormal numbers of new NMD targets and so this saturated capacity of NMD de-represses natural NMD targets. (**B**) De-repression of two known natural NMD targets (*atxn1b* and *mmp30*) in *upf1* morphants (wt-*upf1* MO) and *eftud2*^{fn10a} mutants (mt) compared with wild-type siblings (wt) or wild-type siblings injected with *upf1* mRNA (wt-*upf1* mRNA); the elevated expression of *atxn1b* and *mmp30* was reversed by upf1 mRNA injection in eftud2^{fn10a} mutants ($n \geq 3$). (**C**) Exon-skipped transcripts (lower bands) of *mier1a*, *mlh1* and *ttc8* accumulated in the cytoplasm of *eftud2* morphants at 36 hpf; and the percentage of defective transcripts decreased in *eftud2* morphants over-expressing *upf1* mRNA. (**D**) Statistics of the exon-skipping ratios of *mier1a*, *mlh1,* and *ttc8* in wild-type control (wt con), *eftud2* morphants and *eftud2* morphants with *upf1* mRNA injection at 36 hpf. (**E**) Retained introns of *card9*, *her4.2* and *ube2ia* accumulated in the cytoplasm of *eftud2* morphants at 36 hpf; these were decreased in *eftud2* morphants with *upf1* mRNA injection. *P <0.05; **P <0.01; ***P <0.001 (t-test).

fn10a mutants and wild-type embryos, and these genes were enriched in two KEGG pathways, the spliceosome and the p53 signaling pathway (Figure 7A,B). qRT-PCR assays further validated the increased expression of seven genes in the p53 pathway (Figure 7C).

We then asked whether the activated p53 pathway indeed contributed to neuronal apoptosis in *fn10a* mutants. Knockdown of p53 with an antisense p53 MO partly or completely suppressed the apoptotic neural progenitors in *fn10a* mutants (Figure 7D). Half of the *fn10a* mutant embryos (25/50) had no apoptosis signal and most of the rest (21/50) had a reduced signal, suggesting p53-dependent apoptosis in this mutant.

We next sought methods to rescue or at least alleviate the 'IR/ES transcript stress' by removing the transcripts as much as possible. As previously described, over-expression of *upf1* partially activates the NMD system (59). At the level of 230 pg/embryo, injection of *upf1* mRNA raised its ectopic expression level to 15- to 50-fold that in wild-type embryos (data not shown). Indeed, over-expression of *upf1* by injection of *upf1* mRNA into *eftud2* morphants was able to suppress p53 activation (Figure 7E), suggesting that a compromised NMD mechanism at least partly contributed to the presence of large amounts of IR/ES transcripts. Considering the proportion of IR/ES transcripts between cytoplasm and nucleus (Supplementary Figures S10 and S11), we found a partial rescue in mutants over-expressing *upf1*, since NMD cannot eradicate IR/ES transcripts in the nucleus. In summary, we propose that the non-degraded aberrant transcripts impose particular stress on neural progenitors, activate the p53 signaling pathway, and then promote apoptosis.

DISCUSSION

In this study, we identified the defective gene *eftud2* in the zebrafish *fn10a* mutant by positional cloning, and demonstrated that this mutation led to the abnormal accumulation of mitotic neural progenitors and their apoptosis, while *eftud2* was broadly expressed before 36 hpf but enriched in the CNS later in development. Further RNA-seq and functional analyses revealed that the presence of large numbers of aberrant IR/ES transcripts and activation of the p53 pathway contributed to neural apoptosis in this mutant. This work is consistent with a recent descriptive report on neuronal apoptosis in a TALEN-induced *eftud2* mutant in zebrafish (61), but our work has gained molecular insights into how a general mRNA splicing factor plays a rather restricted role in neural progenitor development by mod-

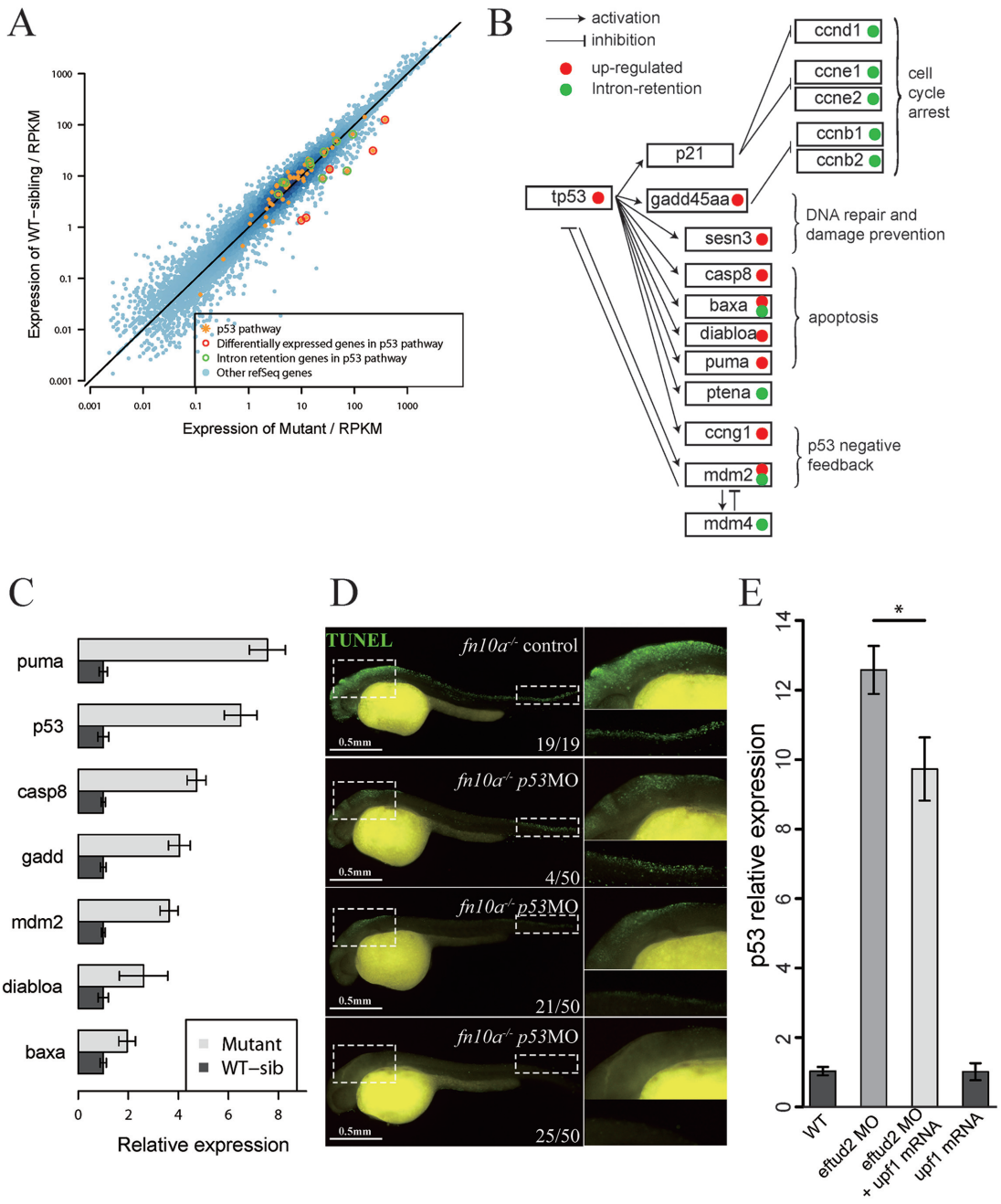

Figure 7. The p53 signaling pathway is activated in *fn10a* mutants. (**A**) Gene expression in RPKM (Reads Per Kilobase of transcript per Million mapped reads) in mutants and WT-siblings. Yellow asterisks, p53 pathway genes; red circles, genes of the p53 pathway differentially expressed in mutants and their siblings; green circles, intron-retained genes in the p53 pathway; and blue circles, other RefSeq genes. (**B**) Genes of the p53 pathway were up-regulated and enriched with intron retention but few had both intron retention and increased mRNA levels in *fn10a* mutants. (**C**) Real-time PCR confirmed the transcriptional up-regulation of p53 pathway genes ($n = 5$). (**D**) Knockdown of p53 expression in *fn10a* mutants rescued neuronal apoptosis in the CNS and spinal cord. Note that ∼50% of p53MO-injected *fn10a* mutants had no TUNEL signals and ∼42% had fewer TUNEL signals. (**E**) Over-expression of *upf1* mRNA partially reduced p53 expression in *eftud2* morphants while it had no effect on p53 expression in wild-type embryos ($n = 5$).

ulating RNA splicing and p53-dependent apoptosis. Taken together, we have not only determined the function of *eftud2* in neural progenitor development but have also established a suitable vertebrate model for further deciphering the molecular pathology of MFDGA caused by haploinsufficiency of EFTUD2.

Since the majority of genes in vertebrates have multiple exons, improper splicing would lead to cellular dysfunction and various disease states. Disruption of either a particular splicing boundary or malfunctional splicing machinery are closely linked with pathological conditions (62–64). MFDGA (OMIM number 610536) is also called mandibulofacial dysostosis with microcephaly (65).

MFDGA patients suffer mainly from craniofacial and neurological defects, and from other developmental issues at lower frequencies. Mutations in EFTUD2 were initially found in these patients through whole-exome sequencing (17), and more have been identified (15,16,66). However, it was not clear how mutations of EFTUD2 in MFDGA cause craniofacial and neurological abnormalities.

Here, we found that *eftud2* was broadly expressed in zebrafish at earlier stages (before 36 hpf), and then was highly concentrated in the brain, consistent with previous reports that *Eftud2* is highly expressed in the ventricular zone of the forebrain of mouse embryos (15) and *eftud2* is enriched in the brain in zebrafish (61). The ventricular zone of the forebrain harbors numerous neural progenitor cells, suggesting an essential role of Eftud2 in CNS development. In zebrafish *eftud2*^{fn10a} mutants, mutation of the human ortholog of *eftud2* leads to primary apoptosis and abnormal proliferation of Sox2^{+} and Ngn1^{+} neuronal progenitors, and a subsequent deficiency of differentiated neurons. Neurons are generated from self-renewing progenitors residing in the ventricular zone of the developing CNS (24,67). Sox2 is restricted to neural progenitors and is essential for maintaining the cell fate of neuronal progenitors, since inhibition of Sox2 compromises neural progenitor differentiation (27,68). In this study, Sox2 was broadly expressed in the neural tube but not restricted to the ventricular zone during development, suggesting that the fate and differentiation of neural progenitors were abolished in *fn10a* mutants, which could explain the increased concentration of mitotic Sox2^{+} neuronal progenitors in the CNS of this mutant. The delayed brain development in *fn10a* mutants is likely due to disruption of neuronal differentiation from progenitors. Therefore, we have established an animal model, the zebrafish *eftud2*^{fn10a} mutant, and determined the function of *eftud2* in neuronal development. Our work provides the first experimental evidence of *eftud2* function in apoptosis and proliferation of neural progenitors, and this serves as a guide for further determining how mutation of EFTUD2 causes neurological phenotypes in MFDGA patients.

p53 plays an important role in the balance between neuronal proliferation and cell death during development (69). Here, we have shown that p53-dependent cell death of neural progenitors is caused by *eftud2* deficiency in zebrafish *fn10a* mutants. On the other hand, we found a broad transcriptional increase of p53 in *fn10a* mutant embryos by whole-mount RNA *in situ* analysis (data not show). Therefore, we were puzzled by why only the CNS responds to the up-regulation of p53 in *fn10a* mutants. Our data show that some IR transcripts such as *ccnb1* and *tardbp* are enriched in the mutant brain, consistent with its defects in the CNS. Several studies have shown that neural progenitors are highly sensitive to apoptosis in a p53-dependent manner (70–72). Previous studies on splicing factors have also demonstrated that mutations of some core spliceosomal factors lead to tissue-specific defects, especially in p53-dependent cell death in the CNS (42,73–78). However, the underlying mechanism has yet to be addressed.

Previous studies have identified many mutations in components or regulators of spliceosomes which can cause abnormal transcriptomes and mutant phenotypes (79–81). In *fn10a* mutants, we found a transcriptome-wide decrease in splicing efficiency (intron retention and exon skipping), making them harder to remove. The consequence was not universal among introns but made a specific set more difficult to splice out. The severely-retained introns tended to be shorter and had a higher GC content. It has been reported that RNA Pol II pausing might contribute to IR since RNA Pol II and spliceosomes compete for space (82). As a higher GC content can hinder the speed of RNA Pol II elongation and so intensify the competition, a shorter intron length would worsen the scenario. Besides, RNA Pol II pauses to wait for checkpoint signals at 3′ splicing sites (83), therefore a weaker 3′ splicing strength would decrease splicing efficiency, making the checkpoint even tougher. This 'intron retention code' is consistent with a recent study on naturally-retained introns in human cells (56), suggesting a tendency toward retention for a large proportion of introns, which could be unleashed when the spliceosome is disturbed. The genes containing severely-retained introns also have several characteristics as they are enriched in the cell cycle, the p53 pathway, and the spliceosome. In addition to IR, a set of genes in the p53 pathway is also differentially expressed, highlighting a crucial role of activation of this pathway, due to splicing deficiency and IRs, and subsequently causing *fn10a* mutant phenotypes, such as apoptosis in the CNS.

For a long time, IR has been taken as a rare form of alternative splicing (45). However, a recent study has identified widespread IRs at the level of half of all introns in the human and mouse genomes, supporting the notion that IR plays an important role in regulating the transcriptome (56). Functionally, IR regulates several biological processes, such as granulocyte differentiation and neuronal development (46,55). By inducing premature stop codons into transcripts, IR often makes mRNA vulnerable to the NMD mechanism, which degrades the mRNA to prevent the production of truncated or malformed proteins. The magnitude of NMD has been reported to decrease during neural development, permitting the increased expression of several natural NMD targets and then undergoing a cell-fate transition from proliferation to differentiation (41,84). In zebrafish, knocking down any of the main components of the NMD machinery leads to abnormal development, including necrosis and apoptosis in the brain (38,60). We thus speculate that the CNS is more susceptible to NMD defects. When *eftud2* is mutated in *fn10a*, the globally-affected transcriptome has major effects on the most vulnerable organ, the CNS, and leads to neuronal apoptosis. The partial suppression of p53 by over-expression of *upf1* in *fn10a* mutants suggests a potential link from splicing deficiency, through IR/ES, to p53 activation. Regarding the relatively modest effect of over-expressed *upf1* on p53 expression, it is also possible that modest activation of the NMD system by merely over-expressing *upf1* and NMD-independent mechanism(s) could also be involved in the regulation. The data for partial rescue (Figure 7E), together with the case studies (Figure 6C–E), suggest an association between abnormal splicing, NMD, and the p53 pathway. Therefore, controlling the level of IR/ES transcripts by enhancing splicing efficiency or NMD capacity deserves exploration as a potential intervention for MFDGA patients.

SUPPLEMENTARY DATA

Supplementary Data are available at NAR Online.

ACKNOWLEDGEMENTS

The authors thank Dr I.C. Bruce for reading the manuscript, Dr Jiulin Du (Shanghai Institute for Biological Sciences) for providing the gfap-GFP1 plasmid clone, and members of the laboratories of Drs Jing-Wei Xiong and Chuanyun Li for helpful discussions and technical assistance.

Authors contributions: L.L. performed most of the experiments, analyzed data, and wrote the manuscript; S.Y.Y., J.C. and C.Y.L. designed the computational methods and experiments for RNA splicing, analyzed data, and wrote the manuscript; R.Y., N.C., Y.B., Q.Z. and X.Z. contributed reagents and performed confocal imaging and cryosections; J.W.X. conceived and designed this study, analyzed data and wrote the manuscript.

FUNDING

National Key Basic Research Program of China [2012CB944501, 2010CB529503, 2013CB531202]; National Natural Science Foundation of China [31430059, 81470399, 31221002, 31271549, 81270164, 31522032]; Funding for open access charge: National Natural Science Foundation of China [31430059, 81470399, 31221002, 31271549, 81270164, 31522032]; National Key Basic Research Program of China [2012CB944501, 2010CB529503, 2013CB531202].

Conflict of interest statement. None declared.

REFERENCES

1. Nilsen,T.W. (2003) The spliceosome: the most complex macromolecular machine in the cell? *BioEssays*, **25**, 1147–1149.
2. Will,C.L. and Luhrmann,R. (2011) Spliceosome structure and function. *Cold Spring Harb. Perspect. Biol.*, **3**, a003707.
3. Schweingruber,C., Rufener,S.C., Zund,D., Yamashita,A. and Muhlemann,O. (2013) Nonsense-mediated mRNA decay—mechanisms of substrate mRNA recognition and degradation in mammalian cells. *Biochim. Biophys. Acta*, **1829**, 612–623.
4. Culbertson,M.R. and Neeno-Eckwall,E. (2005) Transcript selection and the recruitment of mRNA decay factors for NMD in saccharomyces cerevisiae. *RNA*, **11**, 1333–1339.
5. Drechsel,G., Kahles,A., Kesarwani,A.K., Stauffer,E., Behr,J., Drewe,P., Ratsch,G. and Wachter,A. (2013) Nonsense-mediated decay of alternative precursor mRNA splicing variants is a major determinant of the arabidopsis steady state transcriptome. *Plant Cell*, **25**, 3726–3742.
6. Nicholson,P., Yepiskoposyan,H., Metze,S., Zamudio Orozco,R., Kleinschmidt,N. and Mühlemann,O. (2010) Nonsense-mediated mRNA decay in human cells: mechanistic insights, functions beyond quality control and the double-life of NMD factors. *Cell. Mol. Life Sci.*, **67**, 677–700.
7. Schneider,C., Will,C.L., Makarova,O.V., Makarov,E.M. and Luhrmann,R. (2002) Human U4/U6.U5 and U4atac/U6atac.U5 Tri-snRNPs Exhibit Similar Protein Compositions. *Mol. Cell. Biol.*, **22**, 3219–3229.
8. Tarn,W.Y. and Steitz,J.A. (1996) A novel spliceosome containing U11, U12, and U5 snRNPs excises a minor class (AT-AC) intron in vitro. *Cell*, **84**, 801–811.
9. Turner,I.A., Norman,C.M., Churcher,M.J. and Newman,A.J. (2004) Roles of the U5 snRNP in spliceosome dynamics and catalysis. *Biochem. Soc. Trans.*, **32**, 928–931.
10. Fabrizio,P., Laggerbauer,B., Lauber,J., Lane,W.S. and Lührmann,R. (1997) An evolutionarily conserved U5 snRNP-specific protein is a GTP-binding factor closely related to the ribosomal translocase EF-2. *EMBO J.*, **16**, 4092–4106.
11. Frazer,L.N., Nancollis,V. and O'Keefe,R.T. (2008) The role of Snu114p during pre-mRNA splicing. *Biochem. Soc. Trans.*, **36**, 551–553.
12. Brenner,T.J. and Guthrie,C. (2005) Genetic analysis reveals a role for the C terminus of the saccharomyces cerevisiae GTPase Snu114 during spliceosome activation. *Genetics*, **170**, 1063–1080.
13. Voigt,C., Mégarbané,A., Neveling,K., Czeschik,J., Albrecht,B., Callewaert,B., von Deimling,F., Hehr,A., Falkenberg,S.M., König,R. *et al.* (2013) Oto-facial syndrome and esophageal atresia, intellectual disability and zygomatic anomalies - expanding the phenotypes associated with EFTUD2 mutations. *Orphanet J. Rare Dis.*, **8**, 110.
14. Gandomi,S.K., Parra,M., Reeves,D., Yap,V. and Gau,C.L. (2015) Array-CGH is an effective first-tier diagnostic test for EFTUD2-associated congenital mandibulofacial dysostosis with microcephaly. *Clin. Genet.*, **87**, 80–84.
15. Gordon,C.T., Petit,F., Oufadem,M., Decaestecker,C., Jourdain,A.S., Andrieux,J., Malan,V., Alessandri,J.L., Baujat,G., Baumann,C. *et al.* (2012) EFTUD2 haploinsufficiency leads to syndromic oesophageal atresia. *J. Med. Genet.*, **49**, 737–746.
16. Lehalle,D., Gordon,C.T., Oufadem,M., Goudefroye,G., Boutaud,L., Alessandri,J.L., Baena,N., Baujat,G., Baumann,C., Boute-Benejean,O. *et al.* (2014) Delineation of EFTUD2 haploinsufficiency-related phenotypes through a series of 36 patients. *Hum. Mutat.*, **35**, 478–485.
17. Lines,M.A., Huang,L., Schwartzentruber,J., Douglas,S.L., Lynch,D.C., Beaulieu,C., Guion-Almeida,M.L., Zechi-Ceide,R.M., Gener,B., Gillessen-Kaesbach,G. *et al.* (2012) Haploinsufficiency of a spliceosomal GTPase encoded by EFTUD2 causes mandibulofacial dysostosis with microcephaly. *Am. J. Hum. Genet.*, **90**, 369–377.
18. Luquetti,D.V., Hing,A.V., Rieder,M.J., Nickerson,D.A., Turner,E.H., Smith,J., Park,S. and Cunningham,M.L. (2013) 'Mandibulofacial dysostosis with microcephaly' caused by EFTUD2 mutations: expanding the phenotype. *Am. J. Med. Gene A*, **161**, 108–113.
19. Smigiel,R., Bezniakow,N., Jakubiak,A., Bloch,M., Patkowski,D., Obersztyn,E. and Sasiadek,M.M. (2015) Phenotype analysis of Polish patients with mandibulofacial dysostosis type guion-almeida associated with esophageal atresia and choanal atresia caused by EFTUD2 gene mutations. *J. Appl. Genet.*, **56**, 199–204.
20. Zarate,Y.A., Bell,C. and Schaefer,G.B. (2015) Radioulnar synostosis and brain abnormalities in a Patient With 17q21.31 microdeletion involving EFTUD2. *Cleft Palate Craniofac. J.*, **52**, 237–239.
21. Eisen,J.S. (1991) Developmental neurobiology of the zebrafish. *J. Neurosci.*, **11**, 311–317.
22. Lewis,K.E. and Eisen,J.S. (2003) From cells to circuits: development of the zebrafish spinal cord. *Prog. Neurobiol.*, **69**, 419–449.
23. Gotz,M. and Huttner,W.B. (2005) The cell biology of neurogenesis. *Nat. Rev. Mol. Cell Biol.*, **6**, 777–788.
24. Hollyday,M. (2001) Neurogenesis in the vertebrate neural tube. *Int. J. Dev. Neurosci.*, **19**, 161–173.
25. Guerout,N., Li,X. and Barnabe-Heider,F. (2014) Cell fate control in the developing central nervous system. *Exp. Cell Res.*, **321**, 77–83.
26. Appel,B. (2000) Zebrafish neural induction and patterning. *Dev. Dyn.*, **219**, 155–168.
27. Thiel,G. (2013) How Sox2 maintains neural stem cell identity. *Biochem. J.*, **450**, e1–e2.
28. Bylund,M., Andersson,E., Novitch,B.G. and Muhr,J. (2003) Vertebrate neurogenesis is counteracted by Sox1-3 activity. *Nat. Neurosci.*, **6**, 1162–1168.
29. Wegner,M. and Stolt,C.C. (2005) From stem cells to neurons and glia: a Soxist's view of neural development. *Trends Neurosci.*, **28**, 583–588.
30. Yuan,L. and Hassan,B.A. (2014) Neurogenins in brain development and disease: an overview. *Arch. Biochem. Biophys.*, **558**, 10–13.
31. Schmidt,R., Strähle,U. and Scholpp,S. (2013) Neurogenesis in zebrafish – from embryo to adult. *Neural Dev.*, **8**, 3.
32. Mahler,J. and Driever,W. (2007) Expression of the zebrafish intermediate neurofilament Nestin in the developing nervous system and in neural proliferation zones at postembryonic stages. *BMC Dev. Biol.*, **7**, 89.

33. Nielsen,A.L. and Jørgensen,A.L. (2003) Structural and functional characterization of the zebrafish gene for glial fibrillary acidic protein, GFAP. *Gene*, **310**, 123–132.
34. Ladran,I., Tran,N., Topol,A. and Brennand,K.J. (2013) Neural stem and progenitor cells in health and disease. *Wiley Interdiscip. Rev. Syst. Biol. Med.*, **5**, 701–715.
35. Knapik,E.W., Goodman,A., Ekker,M., Chevrette,M., Delgado,J., Neuhauss,S., Shimoda,N., Driever,W., Fishman,M.C. and Jacob,H.J. (1998) A microsatellite genetic linkage map for zebrafish (Danio rerio). *Nat. Genet.*, **18**, 338–343.
36. Bernardos,R.L. and Raymond,P.A. (2006) GFAP transgenic zebrafish. *Gene Expr. Patterns*, **6**, 1007–1013.
37. Blader,P., Plessy,C. and Strähle,U. (2003) Multiple regulatory elements with spatially and temporally distinct activities control neurogenin1 expression in primary neurons of the zebrafish embryo. *Mech. Dev.*, **120**, 211–218.
38. Wittkopp,N., Huntzinger,E., Weiler,C., Sauliere,J., Schmidt,S., Sonawane,M. and Izaurralde,E. (2009) Nonsense-mediated mRNA decay effectors are essential for zebrafish embryonic development and survival. *Mol. Cell Biol.*, **29**, 3517–3528.
39. Thisse,C. and Thisse,B. (2008) High-resolution in situ hybridization to whole-mount zebrafish embryos. *Nat. Protoc.*, **3**, 59–69.
40. Bu,Y., Su,F., Wang,X., Gao,H., Lei,L., Chang,N., Wu,Q., Hu,K., Zhu,X., Chang,Z. *et al.* (2014) Protein tyrosine phosphatase PTPN9 regulates erythroid cell development through STAT3 dephosphorylation in zebrafish. *J. Cell Sci.*, **127**, 2761–2770.
41. Bruno,I.G., Karam,R., Huang,L., Bhardwaj,A., Lou,C.H., Shum,E.Y., Song,H.W., Corbett,M.A., Gifford,W.D., Gecz,J. *et al.* (2011) Identification of a microRNA that activates gene expression by repressing nonsense-mediated RNA decay. *Mol. Cell*, **42**, 500–510.
42. Linder,B., Dill,H., Hirmer,A., Brocher,J., Lee,G.P., Mathavan,S., Bolz,H.J., Winkler,C., Laggerbauer,B. and Fischer,U. (2010) Systemic splicing factor deficiency causes tissue-specific defects: a zebrafish model for retinitis pigmentosa. *Hum. Mol. Genet.*, **20**, 368–377.
43. Parkhomchuk,D., Borodina,T., Amstislavskiy,V., Banaru,M., Hallen,L., Krobitsch,S., Lehrach,H. and Soldatov,A. (2009) Transcriptome analysis by strand-specific sequencing of complementary DNA. *Nucleic Acids Res.*, **37**, e123.
44. Zhang,S.J., Liu,C.J., Yu,P., Zhong,X., Chen,J.Y., Yang,X., Peng,J., Yan,S., Wang,C., Zhu,X. *et al.* (2014) Evolutionary interrogation of human biology in well-annotated genomic framework of rhesus macaque. *Mol. Biol. Evol.*, **31**, 1309–1324.
45. Wang,E.T., Sandberg,R., Luo,S., Khrebtukova,I., Zhang,L., Mayr,C., Kingsmore,S.F., Schroth,G.P. and Burge,C.B. (2008) Alternative isoform regulation in human tissue transcriptomes. *Nature*, **456**, 470–476.
46. Wong,J.J., Ritchie,W., Ebner,O.A., Selbach,M., Wong,J.W., Huang,Y., Gao,D., Pinello,N., Gonzalez,M., Baidya,K. *et al.* (2013) Orchestrated intron retention regulates normal granulocyte differentiation. *Cell*, **154**, 583–595.
47. Audic,S. and Claverie,J.M. (1997) The significance of digital gene expression profiles. *Genome Res.*, **7**, 986–995.
48. Yeo,G. and Burge,C.B. (2004) Maximum entropy modeling of short sequence motifs with applications to RNA splicing signals. *J. Comput. Biol.*, **11**, 377–394.
49. Gross-Thebing,T., Paksa,A. and Raz,E. (2014) Simultaneous high-resolution detection of multiple transcripts combined with localization of proteins in whole-mount embryos. *BMC Biol.*, **12**, 55.
50. Wang,L., Feng,Z., Wang,X. and Zhang,X. (2010) DEGseq: an R package for identifying differentially expressed genes from RNA-seq data. *Bioinformatics*, **26**, 136–138.
51. Neumann,B., Walter,T., Hériché,J.K., Bulkescher,J., Erfle,H., Conrad,C., Rogers,P., Poser,I., Held,M., Liebel,U. *et al.* (2010) Phenotypic profiling of the human genome by time-lapse microscopy reveals cell division genes. *Nature*, **464**, 721–727.
52. Kabashi,E., Lin,L., Tradewell,M.L., Dion,P.A., Bercier,V., Bourgouin,P., Rochefort,D., Bel Hadj,S., Durham,H.D., Vande Velde,C. *et al.* (2010) Gain and loss of function of ALS-related mutations of TARDBP (TDP-43) cause motor deficits *in vivo*. *Hum. Mol. Genet.*, **19**, 671–683.
53. Metze,S., Herzog,V.A., Ruepp,M.D. and Muhlemann,O. (2013) Comparison of EJC-enhanced and EJC-independent NMD in human cells reveals two partially redundant degradation pathways. *RNA*, **19**, 1432–1448.
54. Brogna,S. and Wen,J. (2009) Nonsense-mediated mRNA decay (NMD) mechanisms. *Nat. Struct. Mol. Biol.*, **16**, 107–113.
55. Yap,K., Lim,Z.Q., Khandelia,P., Friedman,B. and Makeyev,E.V. (2012) Coordinated regulation of neuronal mRNA steady-state levels through developmentally controlled intron retention. *Genes Dev.*, **26**, 1209–1223.
56. Braunschweig,U., Barbosa-Morais,N.L., Pan,Q., Nachman,E.N., Alipanahi,B., Gonatopoulos-Pournatzis,T., Frey,B., Irimia,M. and Blencowe,B.J. (2014) Widespread intron retention in mammals functionally tunes transcriptomes. *Genome Res.*, **24**, 1774–1786.
57. Boutz,P.L., Bhutkar,A. and Sharp,P.A. (2015) Detained introns are a novel, widespread class of post-transcriptionally spliced introns. *Genes Dev.*, **29**, 63–80.
58. Longman,D., Hug,N., Keith,M., Anastasaki,C., Patton,E.E., Grimes,G. and Cáceres,J.F. (2013) DHX34 and NBAS form part of an autoregulatory NMD circuit that regulates endogenous RNA targets in human cells, zebrafish and Caenorhabditis elegans. *Nucleic Acids Res.*, **41**, 8319–8331.
59. Wengrod,J., Martin,L., Wang,D., Frischmeyer-Guerrerio,P., Dietz,H.C. and Gardner,L.B. (2013) Inhibition of nonsense-mediated RNA decay activates autophagy. *Mol. Cell Biol.*, **33**, 2128–2135.
60. Anastasaki,C., Longman,D., Capper,A., Patton,E.E. and Caceres,J.F. (2011) Dhx34 and Nbas function in the NMD pathway and are required for embryonic development in zebrafish. *Nucleic Acids Res.*, **39**, 3686–3694.
61. Deml,B., Reis,L.M., Muheisen,S., Bick,D. and Semina,E.V. (2015) EFTUD2 deficiency in vertebrates: identification of a novel human mutation and generation of a zebrafish model. *Birth Defects Res. A Clin. Mol. Teratol.*, **103**, 630–640
62. Wang,G.S. and Cooper,T.A. (2007) Splicing in disease: disruption of the splicing code and the decoding machinery. *Nat. Rev. Genet.*, **8**, 749–761.
63. Ward,A.J. and Cooper,T.A. (2010) The pathobiology of splicing. *J. Pathol.*, **220**, 152–163.
64. Padgett,R.A. (2012) New connections between splicing and human disease. *Trends Genet.*, **28**, 147–154.
65. Guion-Almeida,M.L., Zechi-Ceide,R., Vendramini,S. and Tabith,J.A. (2006) A new syndrome with growth and mental retardation, mandibulofacial dysostosis, microcephaly, and cleft palate. *Clin. Dysmorphol.*, **15**, 171–174.
66. Need,A.C., Shashi,V., Hitomi,Y., Schoch,K., Shianna,K.V., McDonald,M.T., Meisler,M.H. and Goldstein,D.B. (2012) Clinical application of exome sequencing in undiagnosed genetic conditions. *J. Med. Genet.*, **49**, 353–361.
67. Hollyday,M. (2001) Neurogenesis in the vertebrate neural tube.*Int. J. Dev. Neurosci.*, **19**, 161-173.
68. Thiel,G. (2013) How Sox2 maintains neural stem cell identity. *Biochem. J.*, **450**, e1–e2.
69. Medrano,S. and Scrable,H. (2005) Maintaining appearances—The role of p53 in adult neurogenesis. *Biochem. Biophys. Res. Commun.*, **331**, 828–833.
70. D'Sa-Eipper,C., Leonard,J.R., Putcha,G., Zheng,T.S., Flavell,R.A., Rakic,P., Kuida,K. and Roth,K.A. (2001) DNA damage-induced neural precursor cell apoptosis requires p53 and caspase 9 but neither Bax nor caspase 3. *Development*, **128**, 137–146.
71. Katayama,K., Ueno,M., Yamauchi,H., Nagata,T., Nakayama,H. and Doi,K. (2005) Ethylnitrosourea induces neural progenitor cell apoptosis after S-phase accumulation in a p53-dependent manner. *Neurobiol. Dis.*, **18**, 218–225.
72. Semont,A., Nowak,E.B., Silva Lages,C., Mathieu,C., Mouthon,M.A., May,E., Allemand,I., Millet,P. and Boussin,F.D. (2004) Involvement of p53 and Fas/CD95 in murine neural progenitor cell response to ionizing irradiation. *Oncogene*, **23**, 8497–8508.
73. Trede,N.S., Medenbach,J., Damianov,A., Hung,L.H., Weber,G.J., Paw,B.H., Zhou,Y., Hersey,C., Zapata,A., Keefe,M. *et al.* (2007) Network of coregulated spliceosome components revealed by zebrafish mutant in recycling factor p110. *Proc. Natl. Acad. Sci. U.S.A.*, **104**, 6608–6613.
74. Gonzalez-Santos,J.M., Cao,H., Duan,R.C. and Hu,J. (2007) Mutation in the splicing factor Hprp3p linked to retinitis pigmentosa

impairs interactions within the U4/U6 snRNP complex. *Hum. Mol. Genet.*, **17**, 225–239.
75. Kleinridders,A., Pogoda,H.M., Irlenbusch,S., Smyth,N., Koncz,C., Hammerschmidt,M. and Bruning,J.C. (2009) PLRG1 is an essential regulator of cell proliferation and apoptosis during vertebrate development and tissue homeostasis. *Mol. Cell. Biol.*, **29**, 3173–3185.
76. Tanackovic,G., Ransijn,A., Ayuso,C., Harper,S., Berson,E.L. and Rivolta,C. (2011) A missense mutation in PRPF6 causes impairment of pre-mRNA splicing and autosomal-dominant retinitis pigmentosa. *Am. J. Hum. Genet.*, **88**, 643–649.
78. Jia,Y., Mu,J.C. and Ackerman,S.L. (2012) Mutation of a U2 snRNA gene causes global disruption of alternative splicing and neurodegeneration. *Cell*, **148**, 296–308.
77. Keightley,M.C., Crowhurst,M.O., Layton,J.E., Beilharz,T., Markmiller,S., Varma,S., Hogan,B., de Jong-Curtain,T.A., Heath,J. and Lieschke,G.J. (2013) *In vivo* mutation of pre-mRNA processing factor 8 (Prpf8) affects transcript splicing, cell survival and myeloid differentiation. *FEBS Lett.*, **587**, 2150–2157.
79. Markmiller,S., Cloonan,N., Lardelli,R.M., Doggett,K., Keightley,M.C., Boglev,Y., Trotter,A.J., Ng,A.Y., Wilkins,S.J., Verkade,H. *et al.* (2014) Minor class splicing shapes the zebrafish transcriptome during development. *Proc. Natl. Acad. Sci. U.S.A.*, **111**, 3062–3067.
80. Ahn,E.Y., DeKelver,R.C., Lo,M.C., Nguyen,T.A., Matsuura,S., Boyapati,A., Pandit,S., Fu,X.D. and Zhang,D.E. (2011) SON controls cell-cycle progression by coordinated regulation of RNA splicing. *Mol. Cell*, **42**, 185–198.
81. Li,Q., Zheng,S., Han,A., Lin,C.H., Stoilov,P., Fu,X.D. and Black,D.L. (2014) The splicing regulator PTBP2 controls a program of embryonic splicing required for neuronal maturation. *Elife*, **3**, e01201.
82. Braunschweig,U., Gueroussov,S., Plocik,A.M., Graveley,B.R. and Blencowe,B.J. (2013) Dynamic integration of splicing within gene regulatory pathways. *Cell*, **152**, 1252–1269.
83. Alexander,R.D., Innocente,S.A., Barrass,J.D. and Beggs,J.D. (2010) Splicing-dependent RNA polymerase pausing in yeast. *Mol. Cell*, **40**, 582–593.
84. Lou,C.H., Shao,A., Shum,E.Y., Espinoza,J.L., Huang,L., Karam,R. and Wilkinson,M.F. (2014) Posttranscriptional control of the stem cell and neurogenic programs by the nonsense-mediated rna decay pathway. *Cell Rep.*, **6**, 748–764.